

Scaling in the Emergent Behavior of Heavy Electron Materials

N. J. Curro and B.-L. Young

Condensed Matter and Thermal Physics, Los Alamos National Laboratory, Los Alamos, NM 87545, USA

J. Schmalian

Department of Physics and Astronomy and Ames Laboratory, Iowa State University, Ames, Iowa 50011, USA

D. Pines

*Institute for Complex Adaptive Matter, University of California and
Theoretical Division, Los Alamos National Laboratory,
Los Alamos, NM 87545, and Department of Physics,
University of Illinois at Urbana-Champaign, Urbana, IL, 61801, USA*

(Dated: February 8, 2020)

We show that the NMR Knight shift anomaly exhibited by a large number of heavy electron materials can be understood in terms of the different hyperfine couplings of probe nuclei to localized spins and to conduction electrons. The onset of the anomaly is at a temperature T^* , below which an itinerant component of the magnetic susceptibility develops. This second component characterizes the polarization of the conduction electrons by the local moments and is a signature of the emerging heavy electron state. The heavy electron component grows as $\log T$ below T^* , and scales universally for all measured Ce, Yb and U based materials. Our results suggest that T^* is not related to the single ion Kondo temperature, T_K , but rather represents a *correlated* Kondo temperature that provides a measure of the strength of the intersite coupling between the local moments. Our analysis strongly supports the two-fluid description of heavy electron materials developed by Nakatsuji, Pines and Fisk.

PACS numbers: 71.27.+a, 75.20.Hr, 76.60.Cq

A. Introduction

The Kondo lattice is a paradigm for heavy electron materials. Although a complete theoretical description remains elusive after two decades since the discovery of heavy electron behavior, several common experimental signatures have been identified in these materials that must be captured by any theoretical description. In particular, heavy fermion and mixed valent systems exhibit a crossover between localized moments at high temperatures to coherent behavior at low temperatures. Typically this crossover is evident as a broad maximum in the resistivity; in some cases the bulk magnetic susceptibility also exhibits a maximum, although not always at the same temperature as the resistivity. This behavior has traditionally been understood as the onset of coherent scattering of conduction electrons by the Kondo lattice of 4f spins: at high temperatures ($T > T_{\text{coh}}$) the 4f spins scatter the conduction electrons as independent local impurities; however, below T_{coh} and at low temperatures the Kondo lattice behaves in a coherent fashion. Although a microscopic theory of this process has not emerged, experimental signatures of this crossover are clearly evident in many Ce, Yb and U based compounds.

In the majority of heavy electron and mixed valent materials for which Knight shift measurements exist, it has consistently been observed that below a temperature T^* , the NMR (as well as μSR) Knight shift, K , fails to track the bulk susceptibility, χ .^{1,2} The reason for this anomalous behavior has remained elusive. The Knight

shift measures the field at the nucleus brought about by the hyperfine interaction with the electrons. When the electrons are polarized in an external magnetic field, they create a hyperfine field at the nuclei that is proportional to χ . If there is only one magnetic component, then $K \sim \chi$.

Traditionally the breakdown of this relationship has been attributed to local phenomena associated with the 4f electrons. In the crystal field scenario, the hyperfine coupling changes when the excited states of the crystal field split 4f electron become depopulated.³ In the Kondo impurity scenario, T^* is the Kondo temperature, below which the 4f electrons are screened by the conduction electrons and the bulk χ is reduced.⁴ The Knight shift measures the local susceptibility, which is not screened; and therefore the linear relationship between K and χ breaks down. Still other authors have explained this anomaly in terms of a temperature dependent hyperfine coupling that is modified by the onset of coherence.⁵

Here we propose that the origin of this anomaly is collective rather than local, and that T^* is the temperature at which the heavy electron liquid begins to emerge from the Kondo lattice of localized 4f spins. We demonstrate that below T^* the polarization of the background conduction electron spin system by the correlated f -spins is characterized by a distinct and universal temperature dependence. This polarization is characterized by the magnetic susceptibility, $\chi_{\text{cf}} = \langle \mathbf{S}_c \mathbf{S}_f \rangle$, where \mathbf{S}_c and \mathbf{S}_f are the conduction and local moment spins, respectively. We show that the two-fluid description of the Kondo lattice proposed by Nakatsuji, Pines and Fisk (NPF) provides

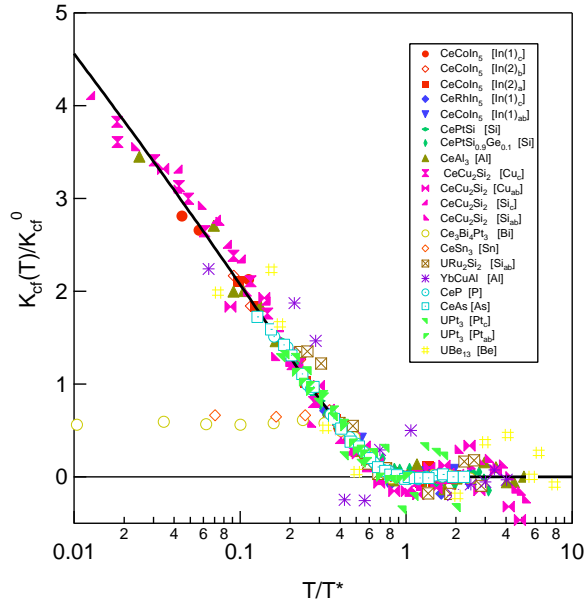


FIG. 1: $K_{cf}(T)/K_{cf}^0$ versus $\ln(T/T^*)$ for several Kondo lattice systems, showing the scaling behavior of the Kondo liquid component of susceptibility. The solid line is given by Eq. (8).

a quantitative explanation for this anomalous behavior.⁶ In turn our analysis allows us to give a more microscopic interpretation for the two fluids introduced by NPF. Our results are consistent with NPF who argued that T^* is a *correlated* Kondo temperature, strongly affected by the intersite f -electron interaction, rather than the familiar single-ion Kondo temperature, T_K . In addition, we are able to determine quantitatively the temperature evolution of the heavy electron spin susceptibility by combining measurements of the temperature dependence of the Knight shift with those of the bulk magnetic susceptibility. We find that an excellent fit to existing experimental data in fourteen heavy electron and mixed valent systems is obtained with a susceptibility whose temperature dependence follows the simple form:

$$\chi_{cf} \sim \left(1 - \frac{T}{T^*}\right) \log \frac{T^*}{T}, \quad (1)$$

a result that suggests that in a Kondo lattice the emergent behavior of the heavy electron liquid can be characterized quite generally by the single energy scale, T^* , that NPF have proposed is a direct measure of the strength of nearest neighbor intersite magnetic coupling. For CeSn_3 and $\text{Ce}_3\text{Bi}_4\text{Pt}_3$ we find quite similar behavior, except that below a cut-off temperature, T_0 , the Knight shift once more tracks the bulk susceptibility. We argue that below T_0 the formation of the heavy electron liquid is complete, and the system has a single, itinerant magnetic component.

In Section B, we discuss the origin of the Knight shift in a Kondo lattice, and its anomalous behavior below

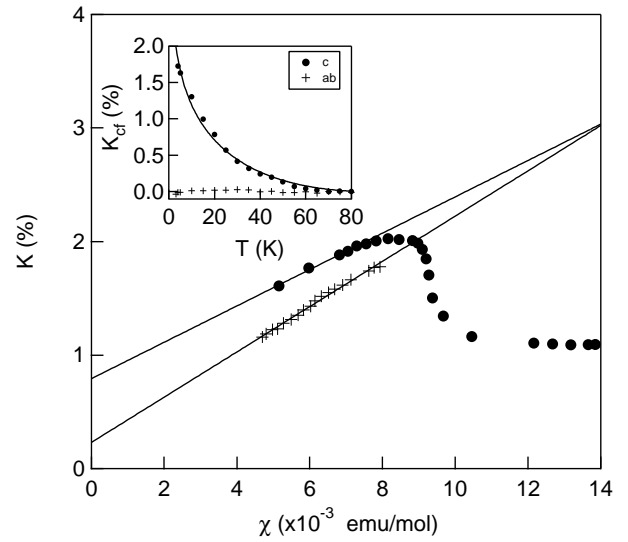


FIG. 2: The In(1) Knight shift in CeCoIn_5 versus the bulk susceptibility.⁷ The solid lines are fits to the high temperature data. Inset: K_{cf} versus T , and a fit to Eq. (8).

T^* in the two-fluid description of NPF. We present the experimental data on fourteen Kondo lattice materials, and show that the simple expression given by Eq. (1) provides a quantitative account of the existing results. For the heavy electron material, CeCoIn_5 , the second component of susceptibility that we obtain by Knight shift measurements is shown to be in excellent agreement with that deduced by NPF. We present our discussion of these results and our conclusions in Section C, and give the data used to obtain our results in the Appendix.

B. Knight Shifts in Kondo Lattice

In the two fluid description proposed by NPF to explain bulk specific heat and susceptibility measurements in La doped CeCoIn_5 , the authors postulate that a fraction $f(T)$ of the 4f electrons in the Kondo lattice become delocalized below T^* , forming a coherent state, the heavy electron liquid, analogous to the superfluid component of ^4He . $f(T)$ resembles an order parameter for the coherent heavy electron component, while the fraction of the 4f (5f) electrons remaining localized resembles the normal fluid component. The magnetic system contains one component that is localized on the magnetic sites i with susceptibility χ_{KI} , and a second component that is associated with the itinerant heavy quasiparticles with susceptibility χ_{HF} :

$$\chi(T) = [1 - f(T)]\chi_{KI}(T) + f(T)\chi_{HF}(T). \quad (2)$$

Detailed insight into the emergence of two contributions to the susceptibility with dramatically different T -dependency can be obtained by taking into account that

the total spin of the system is the sum of the localized f -electron and the conduction electron spins

$$\mathbf{S}_{\text{tot}} = \sum_i \mathbf{S}^f(\mathbf{r}_i) + \sum_l \mathbf{S}^c(\mathbf{r}_l) \quad (3)$$

where \mathbf{r}_i are the positions of the f -electrons and \mathbf{r}_l the positions of the itinerant component of the system within a Wannier orbital representation. $\mathbf{S}^c(\mathbf{r}_l) = \frac{1}{2} \sum_{\sigma\sigma'} c_{\mathbf{r}_l,\sigma}^\dagger \sigma_{\sigma\sigma'} c_{\mathbf{r}_l,\sigma'}$ is the conduction electron spin density. Our results show that at T^* , as a result of the coupling to the f -electron spins, the conduction electrons acquire a heavy component, characterized by the correlation function $\langle \mathbf{S}^f(\mathbf{r}_i) \mathbf{S}^c(\mathbf{r}_l) \rangle$. The uniform susceptibility is now given as $\chi = \frac{1}{N} \frac{\partial}{\partial H} \langle \mathbf{M}_{\text{tot}} \rangle$ where $\mathbf{M}_{\text{tot}} = \sum_i \mathbf{S}^f(\mathbf{r}_i) + \sum_l \mathbf{S}^c(\mathbf{r}_l)$ and it follows that

$$\begin{aligned} \chi &= \chi_{\text{ff}} + 2\chi_{\text{cf}} + \chi_{\text{cc}} \\ &\approx \chi_{\text{ff}} + 2\chi_{\text{cf}}, \end{aligned} \quad (4)$$

where $\chi_{\text{ff}} = \frac{1}{N} \sum_{i,i'} \langle \mathbf{S}^f(\mathbf{r}_i) \mathbf{S}^f(\mathbf{r}_{i'}) \rangle$ and $\chi_{\text{cf}} = \frac{1}{N} \sum_{i,l} \langle \mathbf{S}^f(\mathbf{r}_i) \mathbf{S}^c(\mathbf{r}_l) \rangle$ are the orbital resolved susceptibilities, characterizing the magnetic response of the pure f -system as well as the polarization of the background conduction electron spin system by the correlated f -spins, respectively. We recover the NPF result, Eq. (2), by neglecting χ_{cc} , the uniform susceptibility of the background conduction electrons, which is small, and identifying $\chi_{\text{ff}} = [1 - f(T)]\chi_{\text{KI}}$ and $2\chi_{\text{cf}} = f(T)\chi_{\text{HF}}$.

Quite generally, we expect the hyperfine couplings associated with these two magnetic components to differ. For the local moments, the dominant hyperfine interaction is via a transferred coupling between the nuclei (typically at a different crystalline site) and the local moment. A finite spin density is induced on the neighboring nucleus via wavefunction overlap, or via an indirect interaction mediated by conduction electrons. In general, the transferred hyperfine interaction may couple the nucleus to several nearest neighbor local moment sites. On the other hand, if the magnetic component is delocalized as in a Fermi liquid, it has an additional on-site hyperfine contact term, which generally dominates. For a Kondo lattice system that retains aspects of both localized and delocalized behavior, one can reasonably expect both contact as well as transferred hyperfine couplings. A similar situation is found in the cuprate superconductors.⁸

We therefore postulate the following hyperfine Hamiltonian:

$$\mathcal{H}_{\text{hyp}} = \gamma \hbar \sum_l \mathbf{I}(\mathbf{r}_l) \cdot \mathbf{A} \cdot \mathbf{S}^c(\mathbf{r}_l) + \gamma \hbar \sum_{i,l} \mathbf{I}(\mathbf{r}_l) \cdot \mathbf{B}_i \cdot \mathbf{S}^f(\mathbf{r}_i), \quad (5)$$

where \mathbf{A} and \mathbf{B} are the temperature independent contact and transferred hyperfine tensors, respectively, and \mathbf{r}_i are positions of the nearest neighbor $4f$ ($5f$) sites. The Knight shift is given by: $\mathcal{H}_{\text{hyp}} = \gamma \hbar \sum_l \mathbf{I}(\mathbf{r}_l) \cdot \mathbf{K} \cdot \mathbf{H}_0$, where \mathbf{H}_0 is the applied field. By recognizing that $\langle \mathbf{S}^c(\mathbf{r}) \rangle = \chi_{\text{cf}} \mathbf{H}_0$ and $\langle \mathbf{S}^f(\mathbf{r}) \rangle = (\chi_{\text{cf}} + \chi_{\text{ff}}) \mathbf{H}_0$, and making use of Eqs. (2)

and (5), we then have:

$$K_\alpha(T) = K_{0,\alpha} + (A_\alpha + B_\alpha) \chi_{\text{cf}}(T) + B_\alpha \chi_{\text{ff}}(T) \quad (6)$$

where $K_{0,\alpha}$ is an offset (to account for orbital susceptibility and other T independent effects), and we have dropped the summation over the neighboring sites for simplicity and incorporated the couplings into the constant B . For $T > T^*$, where the linear relationship between Knight shift and bulk susceptibility holds, we make the assumption that $\chi_{\text{cf}}(T) \simeq 0$. This allows us to determine the coupling constant B . In the dilute limit where the single impurity Kondo problem applies, one can carry out an explicit calculation, where indeed one finds for large temperatures ($T \gg T_K$) $\frac{\chi_{\text{cf}}}{\chi_{\text{ff}}} \simeq \rho_F J_K \ll 1$.⁹ Below T^* , $\chi(T)$ and $K_\alpha(T)$ are no longer proportional. $\chi_{\text{cf}}(T)$ and $\chi_{\text{ff}}(T)$ enter into $\chi(T)$ and $K_\alpha(T)$ with different weights, which is due to the additional hyperfine coupling constants in the Knight shift. This allows us to separate the two contributions to the susceptibility from a knowledge of bulk susceptibility and Knight shift. In particular, we obtain the crucial relationship

$$\begin{aligned} K_{\text{cf},\alpha}(T) &= K_\alpha(T) - K_{0,\alpha} - B_\alpha \chi(T) \\ &= (A_\alpha - B_\alpha) \chi_{\text{cf}}(T). \end{aligned} \quad (7)$$

This enables us to single out the heavy electron component, χ_{cf} , that must be thought of as a hybridized many body state where the delocalized nature of the f -spin degrees of freedom is made explicit. We note that a necessary condition for the existence of a Knight shift anomaly is that $A_\alpha \neq B_\alpha$. In Figs. 2 and 4 we show this anomaly in CeCoIn_5 . K_0 and B_α are determined by fitting the high temperature data, shown as the solid lines; these values are given in Table I. Below T^* we obtain the temperature dependence of the heavy electron component, $K_{\text{cf},\alpha}(T)$, which is shown in the inset. Note that without an independent measure of $\chi_{\text{cf}}(T)$, the on-site coupling \mathbf{A} remains undetermined.

In Fig. 1 we plot $K_{\text{cf},\alpha}(T)$ versus T/T^* for fourteen heavy electron and mixed valent systems. T^* is experimentally determined as the temperature below which $\chi(T)$ and $K_\alpha(T)$ cease to be proportional to each other. The collapse of data for such a considerable number of systems is particularly impressive and is the single most important observation of this paper. This universal behavior of χ_{cf} is particularly surprising if one takes into account that the bulk susceptibility χ and the total shift $K_\alpha(T)$ behave qualitatively differently for a number of the compounds shown. It is χ_{cf} which is universal for all these materials.

Based on our observation of universality of χ_{cf} we can now make contact to the two fluid picture of NPF and demonstrate that indeed χ_{cf} agrees with the predictions of their phenomenological approach. In $\text{Ce}_{1-x}\text{La}_x\text{CoIn}_5$, NPF proposed that $\chi_{\text{cf}}(T) = f(T)RC_{\text{cf}}/T$, where R is the Wilson ratio, which successfully explains the doping evolution of the bulk properties. Empirically it was found that $f(T) \sim 1 - T/T^*$, and that $C_{\text{cf}}/T \sim \log(T)$. Combining these results, we arrive at Eq. (1), a candidate

TABLE I: The Knight shift parameters in several Kondo lattice systems.

Material (site) ^{Ref.}	$T^*(K)$	$K_0(\%)$	B_α (kOe/ μ_B)	A_α (kOe/ μ_B)	$K_{cf}^0(\%)$	γ (mJ/mol K ²) ^{Ref.}
CeCoIn ₅ (In(1) _c) ⁷	89	0.79	8.9	13.7	3.3	290 ¹⁰
CeCoIn ₅ (In(1) _{ab}) ⁷	-	0.13	12.1	12.1	-	290 ¹⁰
CeCoIn ₅ (In(2) _a) ⁷	42	1.14	-0.4	-5.9	-2.0	290 ¹⁰
CeCoIn ₅ (In(2) _b) ⁷	42	0.77	10.3	-4.1	-1.3	290 ¹⁰
CeCoIn ₅ (In(2) _c) ⁷	95	-2.43	28.1	12.1	3.1	290 ¹⁰
CeCu ₂ Si ₂ (Cu _c) ³	171	0.04	-0.2	-	-0.3	700 ¹¹
CeCu ₂ Si ₂ (Cu _{ab}) ³	58	-0.05	2.5	-	-0.1	700 ¹¹
CeCu ₂ Si ₂ (Si _c) ³	171	0.12	2.7	-	-0.3	700 ¹¹
CeCu ₂ Si ₂ (Si _{ab}) ³	58	-0.11	8.2	-	-0.2	700 ¹¹
CeRhIn ₅ (In(1) _c)	12	-2.51	26.0	-	1.3	200 ¹²
CeRhIn ₅ (In(1) _{ab})	10	-0.54	19.6	-	2.2	200 ¹²
CeAl ₃ (Al) ¹³	60	0.02	3.5	-	-0.7	1620 ¹⁴
CePtSi (Si) ¹⁵	20	-0.11	7.1	-	-1.7	800 ¹⁶
CePtSi _{0.9} Ge _{0.1} (Si) ¹⁵	15	0.07	4.2	-	-1.4	1350 ¹⁷
CeSn ₃ (Sn) ¹⁸	167	-0.05	32	-	0.2	70 ¹⁹
Ce ₃ Bi ₄ Pt ₃ (Bi) ²⁰	123	0.37	46	-	-1.0	3.3 ²¹
YbCuAl (Cu) ²²	73	0.07	-1.0	-	0.03	260 ²³
URu ₂ Si ₂ (Si _c) ²⁴	84	0.05	3.37	-	-0.03	65 ^{25,26}
CeP (P) ¹	76	0.03	9.98	-	-1.49	17 ²⁷
CeAs (As) ¹	73	0.43	16.3	-	-2.41	?
UPt ₃ (Pt _c) ²⁸	23	3.95	-95.7	-	0.19	420 ²⁹
UPt ₃ (Pt _{ab}) ²⁸	19	-2.0	-54.4	-	1.30	420 ²⁹
UBe ₁₃ (Be) ³⁰	10	-0.02	0.86	-	-0.008	900 ³¹

description of $\chi_{cf}(T)$. Indeed, in the inserts of Figs. 2 and 4 we show fits of $K_{cf}(T)$ to the equation:

$$K_{cf}(T) = K_{cf}^0 \left(1 - \frac{T}{T^*}\right) \log \frac{T^*}{T}, \quad (8)$$

with K_{cf}^0 and T^* as fitting parameters. K_{cf}^0 is given by the value of the shift at $T = \alpha T^*$, where $\alpha \approx 0.259$ is given by the equation $(\alpha - 1) \log \alpha = 1$. Fig. 3 shows K_{cf} versus χ_{cf} in CeCoIn₅, where the χ_{cf} data were extracted from bulk measurements by NPF.^{6,32} The linearity, especially for the *ab* direction, strongly supports the argument that the second component measured by NMR Knight shifts is indeed probing χ_{cf} . Figs. 5 - 14 present comparable data for a number of Ce, Yb and U compounds. In Fig. 1 we show $K_{cf}(T)/K_{cf}^0$ versus T/T^* for all of the materials for which we have thus far been able to obtain Knight shift and susceptibility data. With the exception of Ce₃Bi₄Pt₃, a Kondo insulator, and CeSn₃, a mixed valent system, the data scale remarkably well with one another. This result points to a common mechanism for the Knight shift anomaly, a conclusion that is model independent. In fact, the scaling evident in Fig. 1 is based solely on the reasonable assumption that a second component of susceptibility with a different hyperfine coupling manifests itself below T^* , and that it is this component that exhibits the universal scaling behavior given by Eq. (1). The fact that the scaling form

agrees with the analysis presented by NPF strongly suggests that the two fluid description is relevant for a broad range of heavy fermion materials.

C. Discussion and Conclusions

In Ce₃Bi₄Pt₃ and CeSn₃, the scaling works down to a temperature T_0 , below which K_{cf} saturates. A reasonable explanation is that for these materials $f(T)$ reaches unity at T_0 . Below this temperature, the Kondo liquid is fully formed, and the system has a single, itinerant magnetic component. Furthermore, as seen in Figs. 6 and 11, the linear relationship between K and χ is recovered. In the other heavy fermion systems, both the localized and heavy electron liquid components coexist down to the lowest temperatures measured, typically defined by the onset of magnetic or superconducting order in the particular compounds. Presumably, in the absence of order and for sufficiently low temperatures all the materials should exhibit a saturation. In fact, for CeCu₂Si₂, Fig. 1 suggests that perhaps K_{cf} begins to saturate below $0.02T^* \cong 3.5K$. The distinct T -dependence of χ_{cf} and χ_{ff} below T^* is another strong indication for the fact that T^* is not the single ion Kondo temperature T_K . A collective, rather than local origin of T^* is also supported by the fact that the latter scenario typically leads to the

same T -dependence of χ_{ff} and χ_{cf} below some coherence temperature.³³

For the materials that possess structural symmetries lower than cubic, we note that T^* is anisotropic, in some cases by more than a factor of two. In the two-fluid model of NPF, T^* is a measure of the Ce-Ce intersite coupling. For the bulk measurements presented by NPF, the measured T^* describes an volume average coupling. However NMR results probe a local susceptibility, and the anisotropic T^* 's measured by NMR reflects the anisotropy of the local couplings between the 4f (5f) sites. This anisotropy reflects that of the orbitals that enter the quantum chemistry calculation of the nearest neighbor coupling; in fact the anisotropy might be maximum for directions intermediate to the c and ab planar directions.

We emphasize that the scaling behavior observed by these NMR data strongly support the validity of the two-fluid description in a wide variety of Kondo lattice systems, ranging from heavy electron systems to mixed valent systems. This scaling seems to be independent of the ground state: the materials represented here include magnetically ordered, superconducting, as well as Kondo insulating materials.

The specific heat of the heavy electron fluid of the system was shown by NPF to behave as

$$C_{\text{cf}}(T) = Q \frac{T}{T^*} f(T) \log\left(\frac{T^*}{T}\right) \quad (9)$$

where the dimensionless constant Q determines the entropy contribution of the heavy electron fluid at T^* , $S_{\text{cf}}(T^*) = \int_0^{T^*} \frac{C_{\text{cf}}(T)}{T} dT = \frac{3}{4}Q$. It is natural to assume that $S_{\text{cf}}(T^*)$ is a generic value, independent on the details of the system. Together with the fixed Wilson ratio, $R = \frac{C_{\text{cf}}}{T\chi_{\text{cf}}}$, of the heavy electron component of the two fluid system, this gives

$$\chi_{\text{cf}} = \frac{4}{3R} \frac{S_{\text{cf}}(T^*)}{T^*} f(T) \log\left(\frac{T^*}{T}\right) \quad (10)$$

demonstrating that not only the T -dependence but also the absolute value of χ_{cf} is determined by T^* . In our current analysis, we do not know the hyperfine coupling constant A for all materials and consequently can not determine the prefactor in χ_{cf} . In addition, even if there exists a generic value of $S_{\text{cf}}(T^*)$, this does not, however, imply a universal value for the specific heat coefficient $\gamma = \left. \frac{C(T)}{T} \right|_{T \rightarrow 0}$. A γ -value can only be defined if at some low temperature $T_0 \ll T^*$ the logarithmic growth of $\frac{C_{\text{cf}}(T)}{T}$ stops. Then $\gamma \simeq \frac{Q}{T^*} \log\left(\frac{T^*}{T_0}\right)$ is determined by both T^* and T_0 . Such behavior might reflect, for example, the crossover from a quantum critical regime to a heavy Fermi liquid regime if the system is close to a quantum critical point. As seen in Fig. 17, no correlation between γ and T^* exists. From the NPF perspective, this result is not surprising.

We conclude by noting that for the Cu sites that are nearest to the Fe impurities in the dilute Kondo alloy $\text{Cu}_{1-x}\text{Fe}_x$ there is no Knight shift anomaly.^{34,35} This result supports the argument that the Knight shift anomaly observed in Kondo lattice systems is a *correlated* Kondo effect, determined by the onset of the heavy electron component with a different hyperfine component, rather than a local property of a Kondo screened impurity.

Acknowledgments

This work was performed at Los Alamos National Laboratory under the auspices of the US Department of Energy, and has been supported by the research network on correlated matter of the Institute for Complex Adaptive Matter of the University of California. The authors thank Ar. Abanov, E. Abrahams, F. Borsa, P. Canfield, P. Coleman, D. L. Cox, R. Heffner, F. Hellman, S. Kos, J. Mydosh, S. Nakatsuji, C. P. Slichter, G. Sparn, and Z. Fisk for stimulating discussions.

¹ S. Myers and A. Narath, Solid State Communications **12**(1), 83 (1973).

² D. MacLaughlin, Journal of Magnetism and Magnetic Materials **47-48**, 121 (1985).

³ T. Ohama, H. Yasuoka, D. Mandrus, Z. Fisk, and J. L. Smith, J. Phys. Soc. Jpn. **64**, 2628 (1995).

⁴ E. Kim, M. Makivic, and D. L. Cox, Phys. Rev. Lett. **75**, 2015 (1995).

⁵ J. Sonier, R. Heffner, D. MacLaughlin, J. Smith, J. Cooley, and G. Nieuwenhuys, Physica B **289-290**, 20 (2000).

⁶ S. Nakatsuji, D. Pines, and Z. Fisk, Physical Review Letters **92**(1), 016401/1 (2004).

⁷ N. J. Curro, B. Simovic, P. C. Hammel, P. G. Pagliuso, J. L. Sarrao, J. D. Thompson, and G. B. Martins, Phys. Rev. B **64**, 180514 (2001).

⁸ F. Mila and T. Rice, Physica C **157**(3), 561 (1989).

⁹ V. Barzykin and I. Affleck, Phys. Rev. Lett. **76**, 4959 (1996).

¹⁰ C. Petrovic, P. Pagliuso, M. Hundley, R. Movshovich, J. Sarrao, J. Thompson, Z. Fisk, and P. Monthoux, Journal of Physics: Condensed Matter **13**(17), L337 (2001).

¹¹ F. Steglich, J. Aarts, C. D. Bredl, W. Lieke, D. Meschede, W. Franz, and H. Schäfer, Phys. Rev. Lett. **43**, 1892 (1979).

¹² A. Fisher, F. Bouquet, N. E. Phillips, M. F. Hundley, P. G. Pagliuso, J. L. Sarrao, Z. Fisk, and J. D. Thompson, Phys. Rev. B **65**, 224509 (2002).

¹³ M. Lysak and D. MacLaughlin, Physical Review B (Condensed Matter) **31**(11), 6963 (1985).

¹⁴ K. Andres, J. Graebner, and H. Ott, Physical Review Letters **35**(26), 1779 (1975).

¹⁵ B.-L. Young, Ph.D. thesis, Univ. of Calif., Riverside

- (2003).
- ¹⁶ W. Lee and R. Shelton, Physical Review B (Condensed Matter) **35**(10), 5369 (1987).
 - ¹⁷ F. Steglich, C. Geibel, K. Gloos, G. Olesch, C. Schank, C. Wassilew, A. Loidl, A. Krimmel, and G. Stewart, Journal of Low Temperature Physics **95**(1-2), 3 (1994).
 - ¹⁸ S. K. Malik, R. Vijayaraghavan, S. K. Garg, and R. J. Ripmeester, Physica Status Solidi B **68**, 399 (1975).
 - ¹⁹ C. Stassis, C.-K. Loong, J. Zarestky, O. McMasters, and R. Nicklow, Physical Review B (Condensed Matter) **23**(10), 5128 (1981).
 - ²⁰ A. Reyes, R. Heffner, P. Canfield, J. Thompson, and Z. Fisk, Physical Review B (Condensed Matter) **49**(23), 16321 (1994).
 - ²¹ M. Hundley, P. Canfield, J. Thompson, Z. Fisk, and J. Lawrence, Physical Review B (Condensed Matter) **42**(10), 6842 (1990).
 - ²² D. MacLaughlin, F. de Boer, J. Bijvoet, P. de Chatel, and W. Mattens, Journal of Applied Physics **50**(3 pt.2), 2094 (1979).
 - ²³ W. Mattens, R. Elenbaas, and F. de Boer, Communications on Physics **2**(5), 147 (1977).
 - ²⁴ O. Bernal, B. Becker, J. Mydosh, G. Nieuwenhuys, A. Menovsky, P. Paulus, H. Brom, D. MacLaughlin, and H. Lukefahr, Physica B **281-282**, 236 (2000).
 - ²⁵ T. Palstra, A. Menovsky, J. van den Berg, A. Dirkmaat, P. Kes, G. Nieuwenhuys, and J. Mydosh, Physical Review Letters **55**(24), 2727 (1985).
 - ²⁶ M. Maple, J. Chen, Y. Dalichaouch, T. Kohara, C. Rossel, M. Torikachvili, M. McElfresh, and J. Thompson, Physical Review Letters **56**(2), 185 (1986).
 - ²⁷ Y. Kwon, Y. Haga, O. Nakamura, T. Suzuki, and T. Kasuya, Physica B **171**(1-4), 324 (1991).
 - ²⁸ M. Lee, G. Moores, Y.-Q. Song, W. Halperin, W. Kim, and G. Stewart, Physical Review B (Condensed Matter) **48**(10), 7392 (1993).
 - ²⁹ G. R. Stewart, Z. Fisk, J. O. Willis, and J. L. Smith, Phys. Rev. Lett. **52**, 679 (1984).
 - ³⁰ W. Clark, M. Lan, G. van Kalker, W. Wong, C. Tien, D. MacLaughlin, J. Smith, Z. Fisk, and H. Ott, Journal of Magnetism and Magnetic Materials **63-64**, 396 (1987).
 - ³¹ H. R. Ott, H. Rudigier, Z. Fisk, and J. L. Smith, Physica **127B**, 359 (1984).
 - ³² S. Nakatsuji, private communication (2003).
 - ³³ A. J. Millis and P. A. Lee, Phys. Rev. B **35**, 3394 (1987).

- ³⁴ H. Alloul, Physica **86-88B**, 449 (1977).
- ³⁵ H. Ishii, Physica **86-88B**, 517 (1977).
- ³⁶ J. R. Cooper, C. Rizzuto, and G. Olcese, Journal de Physique **32**(2-3), C1 1136 (1971).
- ³⁷ J. Franse, A. de Visser, A. Menovsky, and P. Frings, Journal of Magnetism and Magnetic Materials **52**(1-4), 61 (1985).

Appendix

Here we include Fig. 3, as well as Figs. 4 through 16, showing the K versus χ relationship, and the anomaly at T^* . The insets of the Figs. show $K_{cf}(T)$, as well as a fit to Eq. (7). In Figs. 18 - 20 we show the bulk susceptibility versus temperature for each compound. T^* is marked with an arrow for each material. Note that the anomalous behavior marking the emergence of the χ_{cf} component is not obvious in the bulk susceptibility; measurements of both the susceptibility as well as the Knight shift are required to identify T^* .

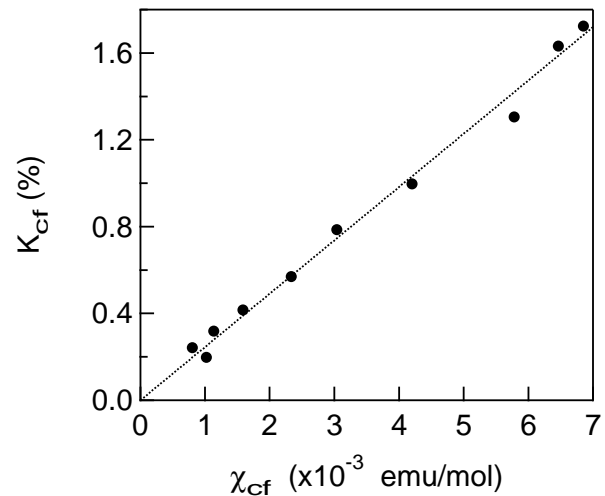


FIG. 3: K_{cf} versus χ_{cf} for CeCoIn₅, where the χ_{cf} were obtained from bulk measurements.³²

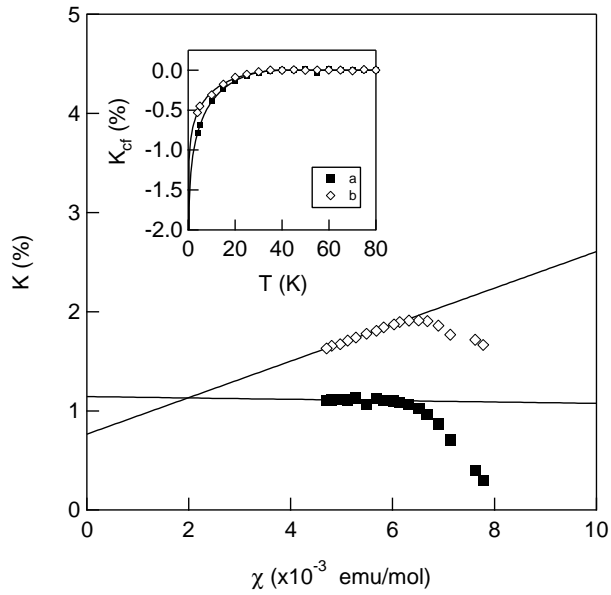


FIG. 4: The In(2) Knight shift CeCoIn_5 versus the bulk susceptibility.⁷ The solid lines are fits to the high temperature data. Inset: K_{cf} versus T , and a fit to Eq. (8).

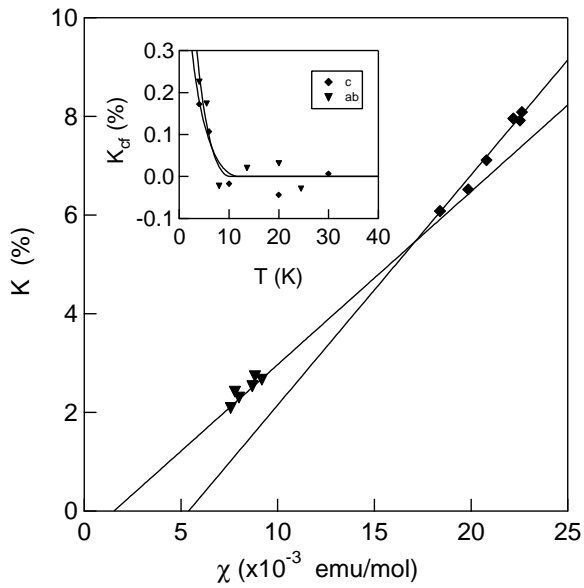


FIG. 5: The In(1) Knight shift in CeRhIn_5 versus the bulk susceptibility. The solid lines are fits to the high temperature data. Inset: K_{cf} versus T , and a fit to Eq. (8).

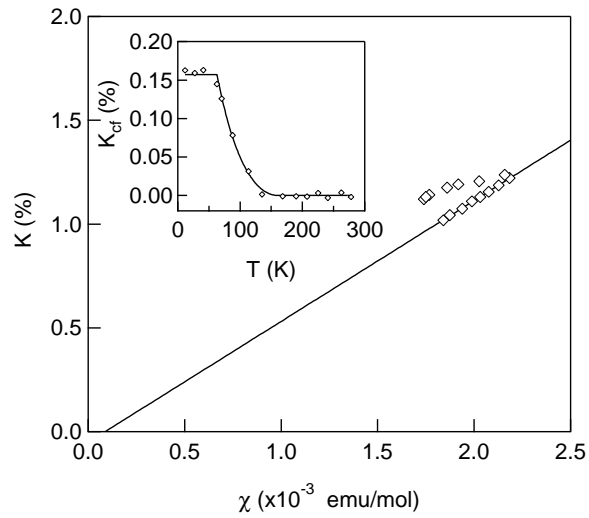


FIG. 6: The Sn Knight shift in CeSn_3 versus the bulk susceptibility.^{18,36} The solid lines are fits to the high temperature data. Inset: K_{cf} versus T , and a fit to Eq. (8).

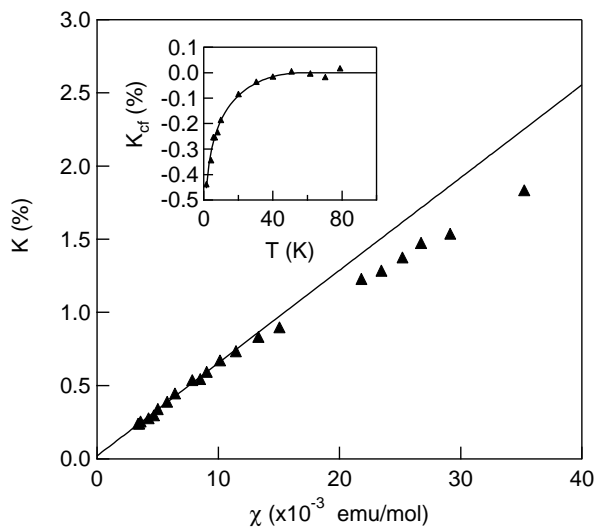


FIG. 7: The Al Knight shift in CeAl_3 versus the bulk susceptibility.¹³ The solid lines are fits to the high temperature data. Inset: K_{cf} versus T , and a fit to Eq. (8).

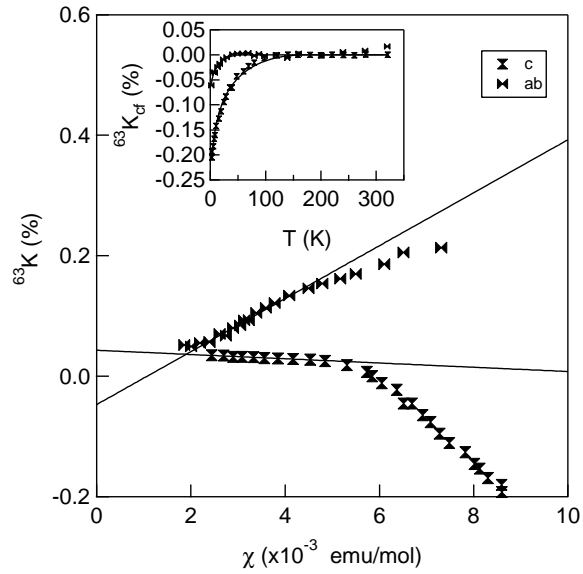


FIG. 8: The Cu Knight shift in CeCu_2Si_2 versus the bulk susceptibility.³ The solid lines are fits to the high temperature data. Inset: K_{cf} versus T , and a fit to Eq. (8).

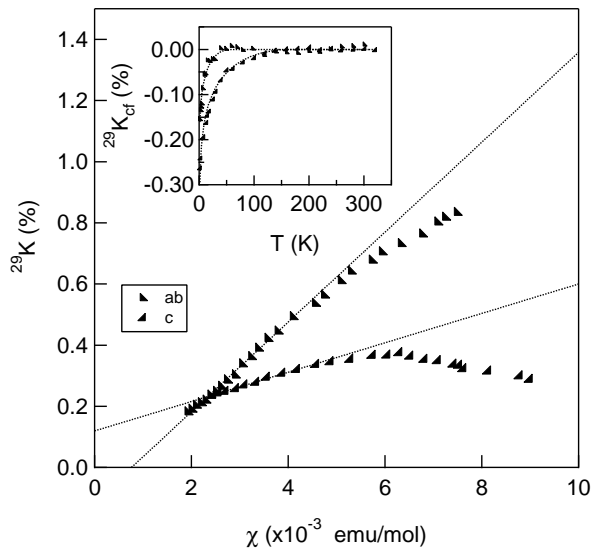


FIG. 9: The Si Knight shift in CeCu_2Si_2 versus the bulk susceptibility.³ The solid lines are fits to the high temperature data. Inset: K_{cf} versus T , and a fit to Eq. (8).

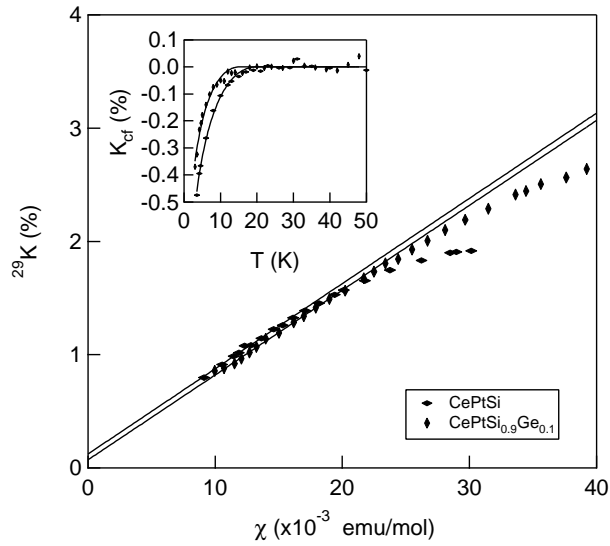


FIG. 10: The Si Knight shift in $\text{CePtSi}_{1-x}\text{Ge}_x$ for $x = 0.0$ and $x = 0.1$ versus the bulk susceptibility.¹⁵ The solid lines are fits to the high temperature data. Inset: K_{cf} versus T , and a fit to Eq. (8).

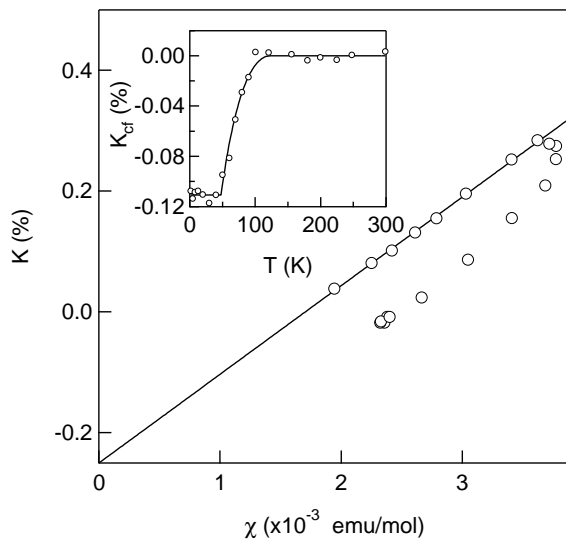


FIG. 11: The Bi Knight shift $\text{Ce}_3\text{Bi}_4\text{Pt}_3$ versus the bulk susceptibility.²⁰ The solid line is a fit to the high temperature data. Inset: K_{cf} versus T , and a fit to Eq. (8).

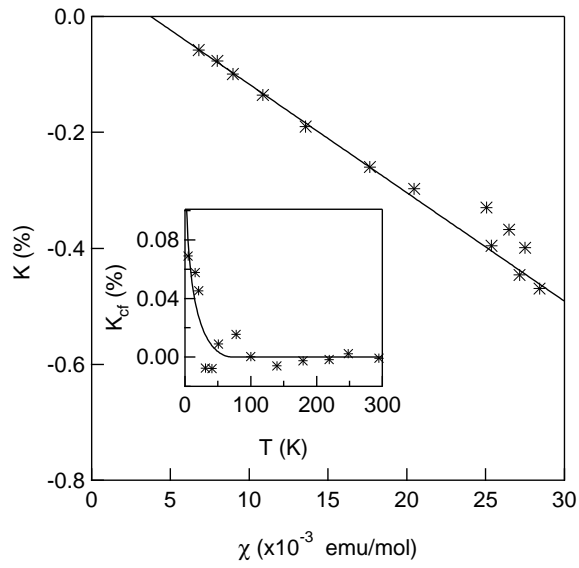


FIG. 12: The Cu Knight shift in YbCuAl versus the bulk susceptibility²². The solid line is a fit to the high temperature data. Inset: K_{cf} versus T , and a fit to Eq. (8).

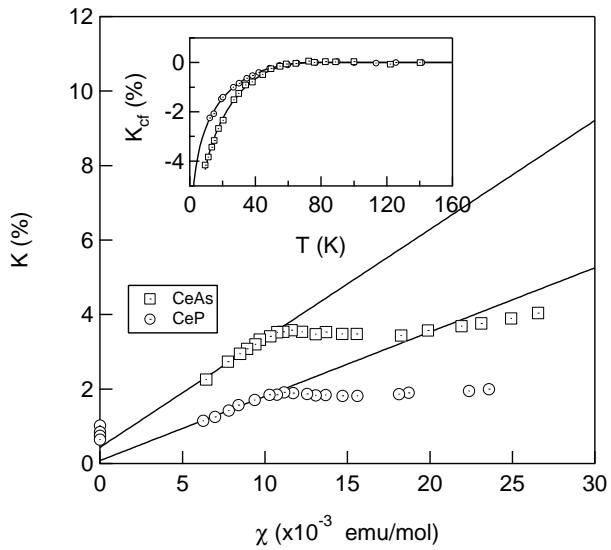


FIG. 13: The P and As Knight shifts in CeP and CeAs versus the bulk susceptibility.¹ The solid line is a fit to the high temperature data. Inset: K_{cf} versus T , and a fit to Eq. (8).

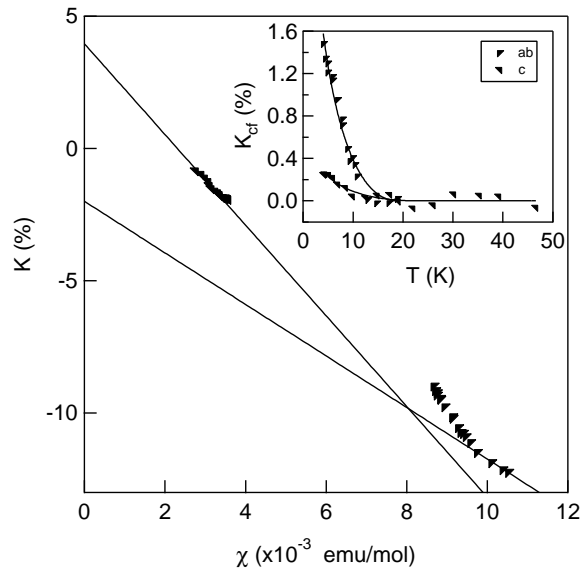


FIG. 14: The Pt Knight shift in UPt_3 versus the bulk susceptibility.^{28,37} The solid line is a fit to the high temperature data. Inset: K_{cf} versus T , and a fit to Eq. (8).

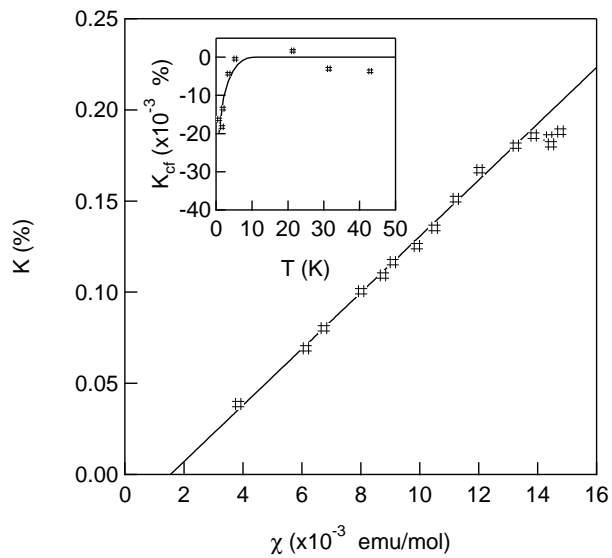


FIG. 15: The Pt Knight shift in UBe_{13} versus the bulk susceptibility.³⁰ The solid line is a fit to the high temperature data. Inset: K_{cf} versus T , and a fit to Eq. (8).

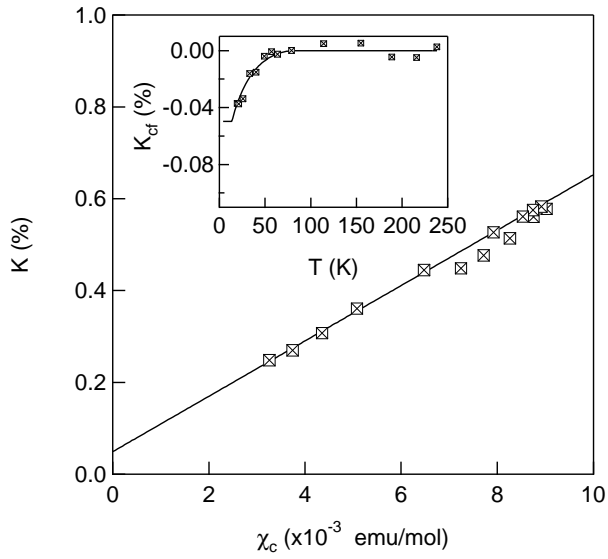


FIG. 16: The Si Knight shift in URu_2Si_2 versus the bulk susceptibility.²⁴ The solid line is a fit to the high temperature data. Inset: K_{eff} versus T , and a fit to Eq. (8).

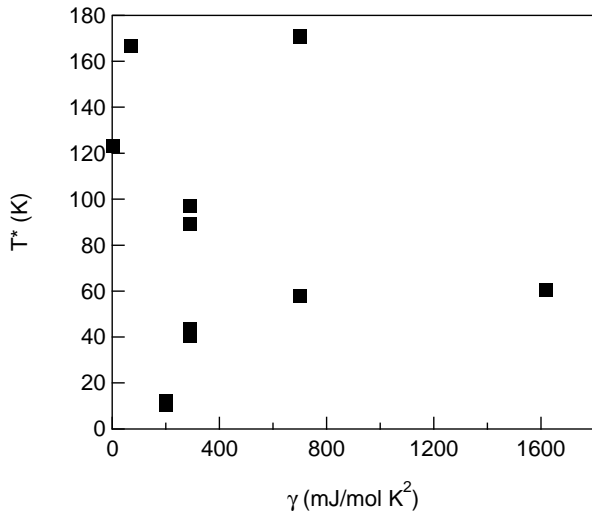


FIG. 17: T^* versus γ for the Kondo lattice systems discussed. There is no apparent correlation.

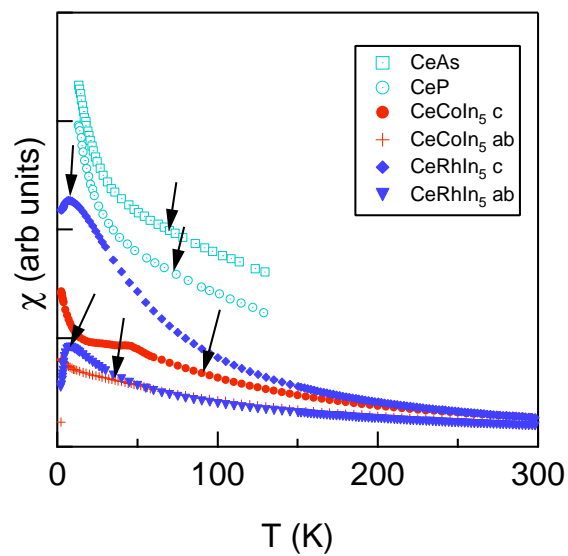


FIG. 18: The susceptibility χ versus temperature in CeAs, CeP, CeCoIn₅, and CeRhIn₅. T^* is marked with an arrow. The data for CeAs and CeP are offset vertically for clarity.

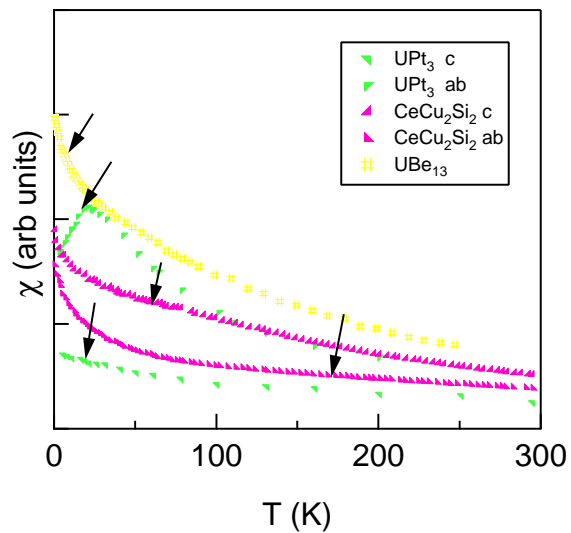


FIG. 19: The susceptibility χ versus temperature in UPt₃, CeCu₂Si₂, and UBe₁₃. T^* is marked with an arrow.

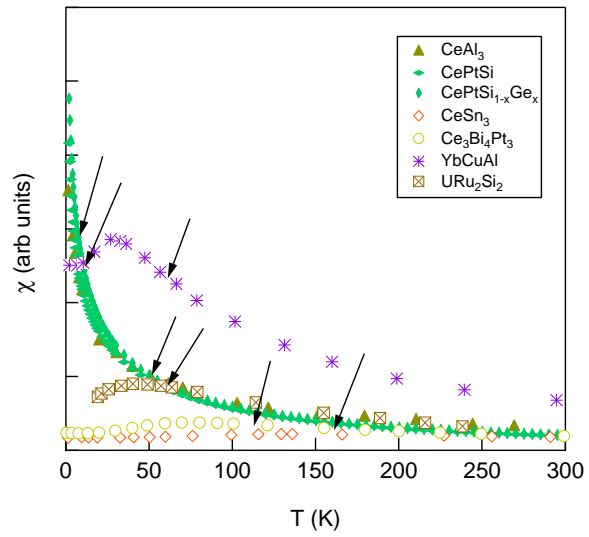


FIG. 20: The susceptibility χ versus temperature in CeAl_3 , $\text{CePtSi}_{1-x}\text{Ge}_x$, CeSn_3 , $\text{Ce}_3\text{Bi}_4\text{Pt}_3$, YbCuAl , and URu_2Si_2 . T^* is marked with an arrow.